optica

Frequency domain Stern–Gerlach effect for photonic qubits and qutrits

Aviv Karnieli[1,*] and Ady Arie[2]

[1]Raymond and Beverly Sackler School of Physics and Astronomy, Tel Aviv University, Ramat Aviv 69978, Tel Aviv, Israel
[2]School of Electrical Engineering, Iby and Aladar Fleischman Faculty of Engineering, Tel-Aviv University, Tel-Aviv, Israel
*Corresponding author: avivkar1@gmail.com

Received 16 July 2018; revised 5 September 2018; accepted 8 September 2018 (Doc. ID 338795); published 16 October 2018

Multi-color photons are prominent candidates for carrying quantum information, as their unlimited dimensionality allows for novel qudit-based schemes. The generation and manipulation of such photons takes place in nonlinear optical media, and the coupling between the different frequency bins can be engineered to obtain the desired quantum state. Here, we propose the design of a frequency-domain Stern–Gerlach effect for photons, where quantum entanglement between the spatial and spectral degrees of freedom is manifested. In this scheme, orthogonal frequency-superposition states can be spatially separated, resulting in a direct projection of an input state onto the frequency-superposition basis. We analyze this phenomenon for two-color qubits and three-color qutrits, and present a generalized wavelength-domain analog of the Hong–Ou–Mandel interference with distinguishable photons. Our results pave the way toward realization of single-element, all-optically controlled spectral-to-spatial beam splitters and tritters that can benefit quantum information processing in the frequency domain. © 2018 Optical Society of America under the terms of the OSA Open Access Publishing Agreement

https://doi.org/10.1364/OPTICA.5.001297

1. INTRODUCTION

Nonlinear optical processes are widely used as platforms for the generation and manipulation of non-classical states of light. Entangled photon pairs and squeezing are the most common examples [1], though much attention has also been given to unitary operations on frequency-domain states [2–10]. Sum-frequency generation (SFG) [2], four-wave mixing [3–7], and electro-optic modulation [8–10] were employed for the dynamic coupling between different frequencies, allowing for high-fidelity spectral-to-spectral (i.e., where both the input and output are in the same spatial mode) quantum gates [10]. The recent interest in these photonic states as quantum information carriers is motivated mainly by their potentially high dimensionality and the ability to transmit them over long distances in optical fibers and in free space. In spite of the growing advancements in this field, quantum effects incorporating the spatial degree of freedom, in a manner that allows for a spatially separated projection on frequency-basis eigenstates, have been rarely explored to date. These *spectral-to-spatial* beam splitters are expected to benefit scalability, particularly when higher dimensional qudits are concerned, since they do not rely on additional optical elements such as frequency converters, waveplates, and dichroic prisms.

In this paper, we demonstrate how paraxial photons in quadratic nonlinear media are analogous to two-dimensional (2D) massive particles carrying internal angular momenta (either spin or orbital). These photons can interact with an external effective field, the components of which are given by the external optical pump fields coupling the different frequencies. For two-level photons, the dynamics coincides with the one described by the Pauli equation for spin-1/2 particles, instead of the usual Schrödinger-type analogy for paraxial propagation. Interestingly, the photon's spectral degree of freedom can become entangled with the spatial ones through a spatial non-uniformity of the nonlinear coupling.

Here, we propose an analogous Stern–Gerlach (SG) effect for photons, which has been recently described for classical light [11]. Such an effect allows for the spatial separation of orthogonal frequency-superposition states, thereby realizing a projection of the quantum state on a different basis otherwise inaccessible within a single nonlinear interaction. We solve analytically for the dynamics and simulate the first-order correlation function of both qubit- and qutrit-photonic states undergoing the aforementioned effect. It is shown that the quantum nature of light is manifested in the form of coherent spatial superposition of the single-photon state as well as two-photon paraxial bunching of the Hong–Ou–Mandel (HOM) type. In contrast to the usual HOM case, here the bunching occurs for photons that are *distinguishable* owing to their different frequencies. The effect proposed herein allows for a realization, using a single optical element, of spectral-to-spatial beam splitters and tritters, all-optically controlled by the pump field, with applications to quantum information processing in the frequency domain.

2. SG EFFECT FOR PHOTONIC QUBITS

For the sake of simplicity, we first treat the case of two-level photonic qubits. The results of this section can, for the most part, be mapped onto the usual polarization subspace of photons that also exhibits SU(2) symmetry. However, it is of great conceptual merit

to discuss them. The crucial difference is that the polarization subspace has only two dimensions, whereas the frequency subspace has unlimited dimensionality. The analysis of effects incorporating two frequencies is merely the most simplified *subset* of the vast variety of manipulations that can be done in this high-dimensional basis. As presented in the following section, these ideas can be readily generalized to effects that couple more than two frequencies.

Consider a quadratic nonlinear medium with a nonlinearity coefficient $\chi^{(2)}$, where a sum-frequency generation (SFG) process takes place. In such media, called nonlinear photonic crystals (NLPCs), the $\chi^{(2)}$ nonlinearity is periodically modulated along the propagation direction with a reciprocal lattice constant $2\pi/\Lambda$, where Λ is the modulation period. The magnitude of Λ is chosen to satisfy the momentum conservation (or *phase matching*) via an umklapp process for a specific three-wave mixing among the frequencies ω_1, ω_2, and $\omega_{12} = \omega_2 - \omega_1$ [12]. We denote the field at frequency ω_{12} as the *pump* field, coupling modes 1 and 2. This pump field will be considered a coherent state that is strong enough that it can be assumed constant throughout the nonlinear interaction. We shall denote $\hbar\kappa_{12} \propto \chi^{(2)}\sqrt{I_{12}}$ (I_{12} being the pump intensity) as the typical coupling energy for the interaction.

The dynamics of the aforementioned model is handled within the paraxial quantum optics formalism [13]. This theory assumes that the electric field operator $E^{(+)}$ can be expressed as a product of a carrier wave $e^{i(k_j z-\omega_j t)}$ and a slowly varying envelope (SVE) operator given for each frequency ω_j by

$$\phi_j(\mathbf{r},t) = \int_Q \frac{\mathrm{d}^3 q}{(2\pi)^3} a(\mathbf{k}_j+\mathbf{q}) e^{i\mathbf{q}\cdot\mathbf{r}-i\delta\omega_j(\mathbf{q})t}. \tag{1}$$

In Eq. (1), $a(\mathbf{k})$ is the usual annihilation operator with $[a(\mathbf{k}), a^\dagger(\mathbf{k}')] = (2\pi)^3\delta(\mathbf{k}-\mathbf{k}')$, $\mathbf{k}_j$ the carrier wavenumber inside the dispersive medium (parallel to the $\hat{z}$ axis), $\delta\omega_j(\mathbf{q}) \equiv \omega(|\mathbf{k}_j+\mathbf{q}|) - \omega_j$, and the integration over $\mathbf{q}$ is restricted to a domain Q satisfying the paraxial approximation [13]. It is straightforward to see that the commutation relation $[\phi_j(\mathbf{r}), \phi_k^\dagger(\mathbf{r}')] = \delta_{jk}\delta(\mathbf{r}-\mathbf{r}')$ holds whenever the different frequencies are spectrally well-separated. Consequently, the paraxial SFG Hamiltonian is written as

$$H_{\mathrm{SFG}} = \int \mathrm{d}^3 r \sum_{j=1,2} \hbar v_{gj} \phi_j^\dagger \left(-i\frac{\partial}{\partial z} - \frac{\nabla_T^2}{2k_j}\right)\phi_j - \int \mathrm{d}^3 r \hbar\kappa_{12}(ie^{i\varphi_{12}}\phi_1^\dagger\phi_2 - ie^{-i\varphi_{12}}\phi_1\phi_2^\dagger), \tag{2}$$

where v_{gj} is the group velocity of the jth frequency, $\nabla_T^2 = \partial_x^2 + \partial_y^2$ is the transverse Laplacian operator, and $\varphi_{12} = -\varphi_{21}$ is a phase associated with the pump field and the NLPC periodicity coupling the modes 1 and 2. The first integral represents paraxial propagation of each wavepacket, while the second integral is the nonlinear part of the Hamiltonian.

The considered wavepackets have a typical temporal length τ. We assume that their propagation is limited to lengths much smaller than the group velocity mismatch (GVM) distance, given by $L_{\mathrm{GVM}} = \tau/|v_{g1}^{-1} - v_{g2}^{-1}|$. Therefore, it is reasonable to neglect the effects of temporal walk-off and consider the different frequencies to travel at some mean group velocity $\bar{v}_g$. We now introduce a spinor notation $\Phi = (\phi_1, \phi_2)^T$ and rewrite our Hamiltonian as

$$H_{\mathrm{SFG}} = \hbar\bar{v}_g \int \mathrm{d}^3 r \Phi^\dagger \left(-i\frac{\partial}{\partial z} + \frac{1}{2}\mathbf{M}^{-1}\mathbf{p}^2 - \Sigma\cdot\mathbf{B}\right)\Phi, \tag{3}$$

where we denote $\mathbf{p} = -i\nabla_T$ as the equivalent momentum operator, and $\mathbf{M}_{ij} = \delta_{ij}k_j$ is the mass matrix (with the carrier wavenumber being the analog of mass). The operator Σ is the Pauli matrices vector, i.e., $\Sigma \equiv (\sigma_x, \sigma_y, \sigma_z)$. The quantity $\mathbf{B}$ is a three-component vector comprised of the different interaction parameters. For this special case, we can define two of the components of $\mathbf{B}$ via the coupling parameters, namely, $B_x = (\kappa_{12}/\bar{v}_g)\cos\varphi_{12}$ and $B_y = (\kappa_{12}/\bar{v}_g)\sin\varphi_{12}$ [14]. A third component, $B_z = \Delta k/2$, emerges when there exists a momentum mismatch $\Delta k = k_2 - k_1 - k_{12} - 2\pi/\Lambda \neq 0$ between the interacting fields.

The system dynamics can be obtained by employing the Heisenberg equation of motion $i\hbar\partial_t\phi_j = [\phi_j, H_{\mathrm{SFG}}]$:

$$i\frac{\partial}{\partial z}\Phi(\mathrm{r},\eta) = \left[\frac{1}{2}\mathbf{M}^{-1}\mathbf{p}^2 - \Sigma\cdot\mathbf{B}(\mathbf{r})\right]\Phi(\mathrm{r},\eta). \tag{4}$$

Note that in Eq. (4) we switched the time t to $\eta = \bar{v}_g t - z$, a coordinate traveling with the wavepacket. At first glance, Eq. (4) is equivalent to the Schrödinger equation for a massive 2D particle, where the propagation coordinate z represents time. This is a well-established analogy for paraxial propagation [15], where, for the case of linear media, the variation in the refractive index is equivalent to a scalar potential. However, in our case, the field considered is vectorial rather than scalar, and is subject to an external coupling $\mathbf{B}$. Since the operator Σ generates SU(2) symmetry, the extended analogy, therefore, is to identify it with an internal angular momentum degree of freedom of spin-1/2. The latter induces the equivalent of a magnetic dipole $\mu \equiv \Sigma$, which in turn interacts with an effective magnetic field $\mathbf{B}$ (we emphasize that this is an analogy, and no actual magnetic field is present). The resulting dynamics is equivalent to the Pauli equation, describing the motion of a spin-1/2 particle in a magnetic field.

The key feature to consider here is that the effective magnetic field $\mathbf{B}$ may vary in space, i.e., $\mathbf{B} = \mathbf{B}(\mathbf{r})$. This is due to the spatial variation of the nonlinear coupling, either induced by the paraxial mode profile of the pump beam, or by spatially varying the nonlinear coefficient. Such variation gives rise to correlations between the spatial and spectral degrees of freedom for single-photon paraxial modes, as will be demonstrated below for the simpler cases of qubits and qutrits.

For two-frequency states, the Bloch sphere representation (Fig. 1) and the role of the SFG process as a rotation of state

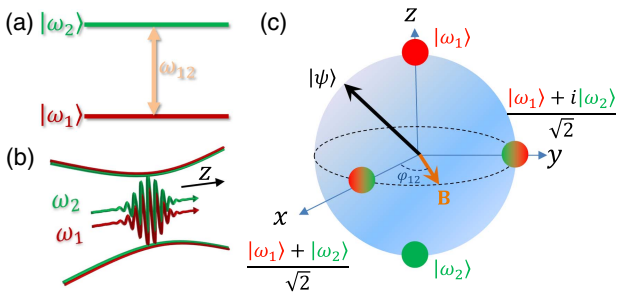

Fig. 1. (a), (b) A two-level photon may occupy two different frequencies, coupled by an external pump field, and have a certain spatio-temporal envelope. (c) The qubit state is represented by a point on the Bloch sphere: pure frequency states are situated on the poles and equal-superposition states lie on the equator. The magnetic field analog, $\mathbf{B}$, was chosen to point to the equator with an angle determined by the pump phase. Hence, the two eigenstates in the direction of $\mathbf{B}$ are superposition states, while the original state $|\psi\rangle$ can be projected onto each of them by employing the proposed SG effect.

vectors have been well established [16,17]. Collinear SFG interactions, together with the dichroic beam splitter, therefore constitute the currently known possible manipulations that can be performed on a two-frequency state: state rotation (analogous to a spectral wave plate), and a projection along the z axis of the Bloch sphere (analogous to a spectral filter), on which lie the pair of pure frequency states $|\omega_i\rangle$ and $|\omega_s\rangle$. It is therefore interesting to ask whether a projection on the Bloch sphere *equator*, hosting the frequency superposition states, is also possible within a single SFG interaction.

Recently, we have studied [11] the all-optical SG effect, in which a classical idler beam ($\omega_1 = \omega_i$) enters into a nonlinear crystal with a transverse gradient in the magnitude of $\mathbf{B}$. This can be achieved in a quasi-phase-matched (QPM) interaction by varying the duty cycle of the periodic poling in the transverse direction, as illustrated in Fig. 2(e) [18]. When such a nonlinear crystal is pumped by a collinear pump wave ($\omega_{12} = \omega_p$), the incident idler beam is deflected into two composite classical states of the signal ($\omega_2 = \omega_s$) and idler frequencies, at positive and negative deflection angles with respect to the optical axis. This is an analog of the SG experiment [19], where a beam of silver atoms carrying an internal spin-1/2 was deflected into two discrete angles by a magnetic field gradient.

The all-optical SG effect is more than an aesthetic analogy between classical wave propagation and quantum mechanics. Recently, it has been proven that universal quantum computation schemes can be based on the $\chi^{(2)}$ interaction [20], where single-qubit gates can be readily realized in the undepleted-pump regime. In this context, a quantum version of the all-optical SG effect greatly simplifies experimental realizations of frequency-domain quantum state projection on the Bloch-sphere equator [Fig. 2(b)], as it requires only a single nonlinear crystal. It is therefore evident that the all-optical SG effect [11] merits a quantum formulation.

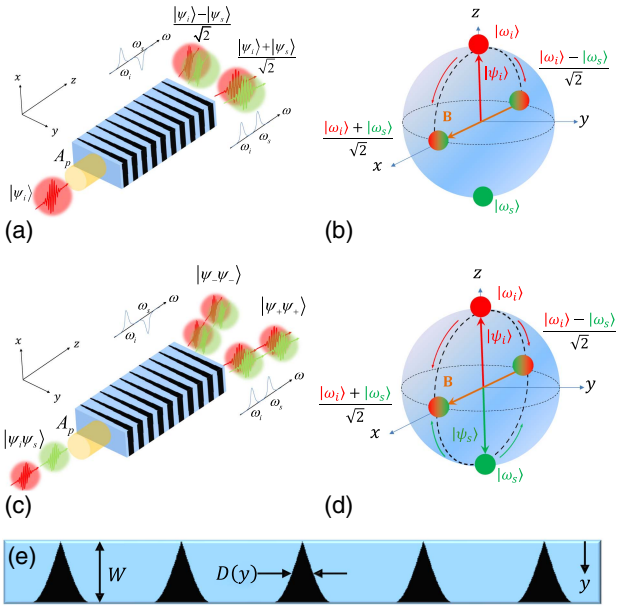

Fig. 2. (a) Single-photon SG interference and (b) its representation on the Bloch sphere. A single-photon wavepacket state in the idler frequency $|\psi_i\rangle$ is incident on a pumped nonlinear SG crystal and transformed into two spatially separated orthogonal frequency superposition single-photon states. (c) Two-photon SG-HOM interference and (d) its representation on the Bloch sphere. Two distinguishable photon wavepacket states are incident on the crystal, and are deflected into a frequency superposition 2002 state, where $|\psi_\pm\rangle = (|\psi_i\rangle \pm |\psi_s\rangle)/\sqrt{2}$. (e) The nonlinearity gradient can be realized by transversely varying the QPM poling duty cycle, D; see Ref. [18].

The analytical solution for the quantum case can be obtained in the following manner. In order to solve Eq. (4) for a linear gradient of the nonlinear coupling in the y direction $\mathbf{B} = (B_0 + B'y)\hat{\mathbf{B}}$, where $\hat{\mathbf{B}} = \hat{\mathbf{x}}\cos\varphi_{12} + \hat{\mathbf{y}}\sin\varphi_{12}$ and $B' \propto \kappa_{12}/W$ [W being the poled region width as in Fig. 2(e)], it is most convenient to transform the spinor Φ to the transverse momentum space. This is a Fourier transformation over the transverse coordinates $\mathbf{r}_T = (x, y)$, given by $\tilde{\Phi}(\mathbf{k}_T, z) = \int \mathrm{d}^2 r_T \Phi \exp(i\mathbf{k}_T \cdot \mathbf{r}_T)$. The transformed field $\tilde{\Phi}$ also happens to represent the far-field operator. In the limit of negligible spatial walk-off, the matrix $\mathbf{M}$ is replaced by a scalar $m \sim \bar{k}$ (where $\bar{k}$ represents a mean wavenumber), and Eq. (4) is diagonalized to the basis of the $\hat{\mathbf{B}}$ direction. Consequently, there exist two eigenfields $\tilde{\Phi}_\pm$ corresponding to the eigenvectors of $\Sigma \cdot \hat{\mathbf{B}}$, which propagate according to their respective eigenvalue:

$$i\frac{\partial}{\partial z}\tilde{\Phi}_\pm = \left[-\frac{\mathbf{k}_T^2}{2\bar{k}} \mp \left(B_0 - iB'\frac{\partial}{\partial k_y}\right)\right]\tilde{\Phi}_\pm. \tag{5}$$

The solution of Eq. (5) is given in terms of propagation operators $\exp(-iH_\pm z)$ acting on each eigenfield $\tilde{\Phi}_\pm$ separately:

$$\begin{aligned}\exp(-iH_\pm z) = &\exp\left(\pm izB_0 - iz^3\frac{B'^2}{6\bar{k}}\right)\\ &\times \exp\left(\mp zB'\frac{\partial}{\partial k_y}\right)\\ &\times \exp\left(-iz\frac{\mathbf{k}_T^2}{2\bar{k}} \mp iz^2\frac{B'k_y}{2\bar{k}}\right).\end{aligned} \tag{6}$$

The first exponential in Eq. (6) is responsible for phase accumulation (both linear and cubic, due to the linear variation of $\mathbf{B}$). The third exponential is the paraxial diffraction with a self-acceleration phase accumulation, also found in Airy beams [21]. The essential property of these operators, however, is the SG deflection part, given by the second exponential:

$$\mathbf{D}(\alpha) = \exp\left(-\alpha\bar{k}\Sigma \cdot \hat{\mathbf{B}}\frac{\partial}{\partial k_y}\right), \tag{7}$$

where in Eq. (7) we have rewritten it in the most general (non-diagonalized) form, so the $\Sigma \cdot \hat{\mathbf{B}}$ term appears inside. The action of this operator results in a deflection of different eigenfields $\tilde{\Phi}_\pm$ by opposite angles, according to the corresponding eigenvalues. The far-field deflection angle for a screen situated outside the nonlinear crystal is given as $\alpha = nB'L/\bar{k}$, where n is the refractive index of the medium, and L the distance traveled inside it. The deflection is governed by the gradient of the nonlinear coupling along y, $B' \propto \kappa_{12}/W$.

This SG effect for two-frequency photonic states is a simple manifestation of quantum correlations between the spatial degrees of freedom and the spectral (internal) ones. We proceed by writing the output field $\tilde{\Phi}_{\mathrm{out}}$ in terms of the original input field $\tilde{\Phi}_{\mathrm{in}} = (\tilde{\phi}_i, \tilde{\phi}_s)^T$ and the unitary transformation $\mathbf{U}$ that diagonalizes $\Sigma \cdot \hat{\mathbf{B}}$, i.e., $\Sigma \cdot \hat{\mathbf{B}} = \mathbf{U}^{-1}\sigma_z\mathbf{U}$ [where $\sigma_z = \mathrm{diag}(1, -1)$ is the third Pauli matrix]. The general expression for $\tilde{\Phi}_{\mathrm{out}}$ is given by

$$\tilde{\Phi}_{\text{out}} = \mathbf{U}^{-1} \exp\left(-\alpha\sigma_z \frac{\partial}{\partial k_y}\right)\mathbf{U}\tilde{\Phi}_{\text{in}}. \tag{8}$$

To further appreciate this relation, we denote the far-field operators as $\tilde{\phi}_R$ and $\tilde{\phi}_L$, the fields deflected to the right and to the left, respectively. This gives us an effective spectral-to-spatial beam splitter relation between the input and output fields:

$$\begin{pmatrix}\tilde{\phi}_R \\ \tilde{\phi}_L\end{pmatrix} = \frac{1}{\sqrt{2}}\begin{pmatrix}1 & e^{i\varphi_{12}} \\ e^{-i\varphi_{12}} & -1\end{pmatrix}\begin{pmatrix}\tilde{\phi}_i \\ \tilde{\phi}_s\end{pmatrix}, \tag{9}$$

where the explicit expression for $\mathbf{U}$ was used in Eq. (9). It is worthwhile to consider here the analogy to polarization. The relation above is very similar to a polarizing beam splitter (PBS), where the polarization direction is controlled by the phase angle φ_{12}. Indeed, under the undepleted pump approximation employed in our analysis, the nonlinear interaction between the two frequencies becomes linear, having an SU(2) symmetry, as is the case with polarization in birefringent media. However, Eq. (9) represents a *frequency-superposition* beam splitter that projects a quantum state from a *single* spatial input port onto orthogonal frequency eigenstates emerging from two output ports.

For simplicity's sake we consider as a test case $\hat{\mathbf{B}} = \hat{x}$, i.e., the phase between the pump wave and the nonlinear modulation pattern is $\varphi_{12} = 0$. (This is an arbitrary choice, whereas a different selection, such as $\varphi_{12} = \pi/2$, would have resulted in the projection of the state along the $\hat{y}$ basis instead [see Fig. 1(c)]. In a practical experiment, two orthogonal transverse bases such as $\hat{x}, \hat{y}$ can always be chosen by varying the pump phase by $\pi/2$.) An incident one-photon state in the idler frequency with a spatial envelope $\psi(r)$, written as $|\psi_{\text{in}}\rangle = |\psi_i\rangle = |\psi(r)\rangle \otimes |\omega_i\rangle$, is then deflected into the output state:

$$|\psi_{\text{out}}\rangle = \frac{1}{\sqrt{2}}\left[\left(\frac{|\psi_i\rangle + |\psi_s\rangle}{\sqrt{2}}\right)_R + \left(\frac{|\psi_i\rangle - |\psi_s\rangle}{\sqrt{2}}\right)_L\right], \tag{10}$$

where $|\psi_s\rangle$ is a state with the same envelope as $|\psi_i\rangle$, but in the signal frequency. A single idler photon, hence, is projected onto an equal and coherent superposition of spatially separated, orthogonal two-frequency states [see Figs. 2(a) and 2(b)]. This projection is unique since the relevant basis lies on the equator of the Bloch sphere.

As a proof of concept, we simulate the propagation of the photodetection amplitude $\psi_j(\mathbf{r}) = \langle 0|\phi_j(\mathbf{r})|\psi_{\text{in}}\rangle$ $(j = i, s)$ and the resulting photodetection probability density $G^{(1)}(\mathbf{r})$ (see Appendix A for details) under realistic experimental conditions. The idler, signal, and pump free-space wavelengths were chosen to be $\lambda_i = 532$ nm, $\lambda_s = 452$ nm, and $\lambda_p = 3000$ nm, respectively. For the nonlinear medium, we chose periodically poled lithium niobate (PPLN) with $d_{33} = 27$ pm/V and QPM period of 6.98 μm (larger periods can be used if the idler wavelength is in the near-infrared). The poled region was designed to induce a transverse gradient in the nonlinear coupling as in Fig. 2(e) (see Ref. [18] and, for further details, Ref. [11]), with a width of $W = 400$ μm and length along the propagation axis of $L = 35$ mm. The pump peak power was $P_p = 1$MW with a waist of 1 mm, giving a peak intensity of roughly $I_p \simeq 64$ MW/cm^2. The simulated input states in the idler and signal frequencies were all Gaussian with a 50 μm waist. Figure 3 presents the propagation and far-field deflection of $G^{(1)}(\mathbf{r})$ for the different input states. The results agree well with the analytic predictions: pure eigenstates are deflected either to the left or to the right, whereas

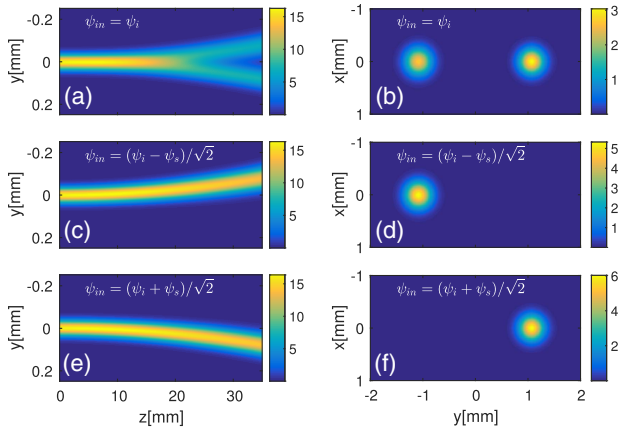

Fig. 3. Simulated photodetection probability in PPLN with a SG poling pattern [with units mm^{-1} on the left figures and mm^{-2} on the right ones, normalized so that the total probability, by integrating over y (left) or xy (right), is 1]. Propagation along the z axis is presented to the left, while the far-field pattern is given to the right. All input states are Gaussian with a waist of 50 μm. (a), (b) The input state is $|\psi_{\text{in}}\rangle = |\psi_i\rangle$ and is deflected into two discrete angles. (c), (d) The input state is an eigenstate $|\psi_{\text{in}}\rangle = (|\psi_i\rangle - |\psi_s\rangle)/\sqrt{2}$, and is deflected only to the left. (e), (f) For the second eigenstate, $|\psi_{\text{in}}\rangle = (|\psi_i\rangle + |\psi_s\rangle)/\sqrt{2}$, the deflection is only to the right.

an idler frequency input is deflected into both angles, since it comprises a superposition of the two eigenstates.

An actual experimental design is expected to be sensitive to the quality and magnitude of the nonlinear coupling gradient. Two significant design considerations are worth mentioning. (i) Phase matching. As stated before, a phase mismatch $\Delta k \neq 0$ between the wavevectors of the interacting photons introduces a z component $B_z \propto \Delta k$ to the effective coupling field $\mathbf{B}$, thus decreasing the magnitude of the transverse (x, y) gradient in $|\mathbf{B}|$. (ii) Nonlinear coupling strength. Stronger nonlinearities and pumps result in larger deflection angles; therefore, it is favorable to use crystals with a relatively high nonlinear coefficient, with PPLN being a good example. For crystals with lower nonlinearity, the design should be compensated, for example, by increasing the pump intensity. Moreover, we note that the duty-cycle-based gradient scheme [Fig. 2(e)] is easier to realize in PPLN than in PPKTP, as the strong anisotropy of the latter crystal tends to align the ferroelectric domain boundaries along the crystal's y axis.

More interesting phenomena involve two-photon interference. We consider an incident state at two different frequencies, $|\psi_{\text{in}}\rangle = |\psi_i\psi_s\rangle$. The corresponding output state is

$$|\psi_{\text{out}}\rangle = \frac{1}{\sqrt{2}}\left[\left(\frac{|\psi_i\rangle + |\psi_s\rangle}{\sqrt{2}}\right)_R^2 - \left(\frac{|\psi_i\rangle - |\psi_s\rangle}{\sqrt{2}}\right)_L^2\right], \tag{11}$$

where the notation $(|\psi\rangle)^2 \equiv |\psi\rangle \otimes |\psi\rangle$ denotes two photons in an identical state. The state $|\psi_{\text{out}}\rangle$ demonstrates paraxial photon bunching: the two photons can only be detected simultaneously in either the left or right part of the spatial mode [see Fig. 2(c)]. Such a state is inherently entangled, and is the simplest example of a NOON state with $N = 2$ for frequency-superposition photons. Further, it is a new manifestation of the only recently observed frequency-domain HOM effect, demonstrated with collinear SFG and a dichroic beam splitter [2], in four-wave mixing [3], and by using the electro-optic effect together with linear optics

[9]. An interesting observation is that this effect occurs only when the two photons are *distinguishable*, as opposed to the original HOM effect, which requires indistinguishable photons. Unlike Refs. [2,3,9], here the entire effect occurs in the nonlinear crystal, saving the need for additional optical elements. Moreover, the resulting projection of the quantum state in these works was limited to the Bloch sphere poles ($|\omega_i\rangle$ and $|\omega_s\rangle$), as opposed to the frequency-superposition scheme presented here.

3. QUTRIT CASE

Next, we discuss the nontrivial case of paraxial photonic qutrits. The internal degree of freedom is now three dimensional, in contrast to the well-known two-state polarization subspace for light. Our analysis for qubits can be easily generalized by inserting a second interaction term between frequencies ω_i and ω_j and with coupling κ_{ij} into Eq. (2):

$$H_{\mathrm{SFG}} = \int \mathrm{d}^3 r \sum_{j=1,2,3} \hbar v_{gj} \phi_j^\dagger \left(-i\frac{\partial}{\partial z} - \frac{\nabla_T^2}{2k_j}\right)\phi_j - \int \mathrm{d}^3 r \hbar \sum_{(jk)} \kappa_{jk}(ie^{i\varphi_{jk}}\phi_j^\dagger \phi_k - ie^{-i\varphi_{jk}}\phi_j \phi_k^\dagger). \quad (12)$$

This is made possible in specially engineered structures called nonlinear photonic *quasi-crystals* (NLPQCs) [22,23], where now the $\chi^{(2)}$ nonlinearity is quasi-periodically modulated along the propagation direction with several fundamental lattice constants $2\pi/\Lambda_l, l = 1, 2, \ldots$ Each Λ_l is chosen to satisfy phase matching for the interaction of ω_i, ω_j and the corresponding pump $\omega_{ij} = \omega_j - \omega_i$. This arrangement allows for two (or more) different nonlinear processes to occur simultaneously.

The dynamics of paraxial qutrits is still given by Eq. (4), with $\Phi = (\phi_1, \phi_2, \phi_3)^T$ and the necessary adjustments for Σ and $\mathbf{B}$, to be discussed shortly. However, there is still freedom in the choice of coupling. The three possible choices are the Λ scheme, the V scheme, and the ladder scheme [see Figs. 4(a)–4(c)]. The operator Σ is again a three-component vector, this time of 3×3 Hermitian matrices $\Sigma_{jk} = iL_{jk}$ [with $(jk) = (12), (23)$ or (31)], where L_{jk} are anti-Hermitian and given by

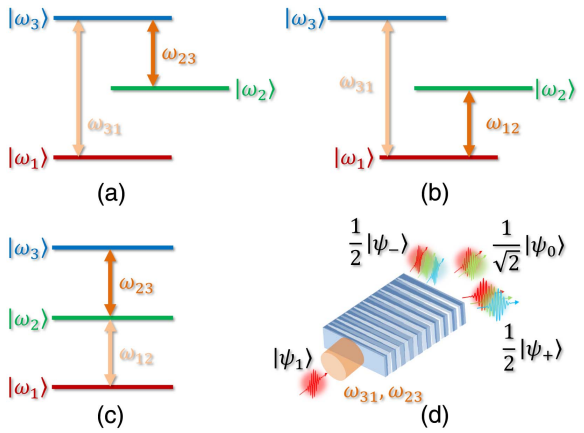

Fig. 4. Three possible configurations for frequency-domain photonic qutrits: (a) Λ scheme, (b) V scheme, and (c) nearest-level (ladder) scheme. (d) Illustration of the SG deflection for a single Λ scheme photon in the lowest frequency $|\psi_{\mathrm{in}}\rangle = |\psi_1\rangle$. The expressions for the eigenstates $|\psi_\pm\rangle$ and $|\psi_0\rangle$ are given in Eq. (16).

$$(L_{jk})_{mn} = e^{i\varphi_{jk}}\delta_{jm}\delta_{kn} - e^{-i\varphi_{jk}}\delta_{jn}\delta_{km}. \quad (13)$$

The matrices L_{jk} form a closed Lie algebra $[L_{jk}, L_{pq}] = L_{jq}\delta_{pk} + L_{pj}\delta_{kq} + L_{qk}\delta_{jp} + L_{kp}\delta_{qj}$, conditioned that the coupling phases satisfy $\varphi_{jk} + \varphi_{kl} = \varphi_{jl}$ for all j, k, l (hence, only two out of three couplings can be present simultaneously). Up to the phase factors, the L_{jk} are identical with the generators of the three-dimensional rotation group SO(3). Namely, we can associate the components of the orbital angular momentum operator, L_x, L_y, and L_z, with the set of matrices L_{23}, L_{31}, and L_{12}, respectively. Similar to the qubit case, an analog of a dipole moment $\mu = \Sigma$ is associated with the internal angular momentum degree of freedom. The three corresponding components of the magnetic field equivalent $\mathbf{B}$ are now simply given by $\mathbf{B}_{jk} = \kappa_{jk}/\bar{v}_g$.

When a transverse coupling gradient is present, we expect that a SG effect [Eqs. (7)–(9)] is manifested in this case, as well. For example, if one chooses to work with the Λ scheme [Fig. 4(a)], the nonvanishing components of the coupling field $\mathbf{B}$ are $B_x = \kappa_{23}/\bar{v}_g$ and $B_y = \kappa_{31}/\bar{v}_g$. We again have $\hat{\mathbf{B}} = \hat{\mathbf{x}}\cos\theta + \hat{\mathbf{y}}\sin\theta$, where this time $\tan\theta = \kappa_{31}/\kappa_{23}$. Each input photon is now projected on the three eigenstates of $\Sigma \cdot \hat{\mathbf{B}}$ and, subsequently, either deflected to distinct angles on the right (R) or on the left (L), or remains undeflected in the middle (M). Consequently, Eq. (9) becomes

$$\begin{pmatrix} \tilde{\phi}_R \\ \tilde{\phi}_M \\ \tilde{\phi}_L \end{pmatrix} = \begin{pmatrix} -\frac{e^{i\varphi_{21}}\sin\theta}{\sqrt{2}} & \frac{\cos\theta}{\sqrt{2}} & \frac{ie^{i\varphi_{23}}}{\sqrt{2}} \\ ie^{i\varphi_{31}}\cos\theta & ie^{i\varphi_{32}}\sin\theta & 0 \\ -\frac{e^{i\varphi_{21}}\sin\theta}{\sqrt{2}} & \frac{\cos\theta}{\sqrt{2}} & -\frac{ie^{i\varphi_{23}}}{\sqrt{2}} \end{pmatrix} \begin{pmatrix} \tilde{\phi}_1 \\ \tilde{\phi}_2 \\ \tilde{\phi}_3 \end{pmatrix}, \quad (14)$$

and one should replace σ_z in Eq. (8) with $S_z = \mathrm{diag}(1, 0, -1)$. Moreover, as in the previous two-level case, the deflection angles can be all optically controlled by the intensity of the pumps. For example, consider an input state $|\psi_{\mathrm{in}}\rangle = |\psi_1\rangle$ (the ket $|\psi_j\rangle = |\psi(r)\rangle \otimes |\omega_j\rangle$ represents a photon in the jth frequency state and with some spatial envelope $\psi(r)$). For simplicity, we factor out all imaginary coefficients in Eq. (14) by setting $\varphi_{23} = \varphi_{31} = -\pi/2$, where it follows that $\varphi_{21} = -\pi$. Another simplification is to take $\theta = \pi/4$, i.e., $\kappa_{23} = \kappa_{31}$. The output state is then given by

$$|\psi_{\mathrm{out}}\rangle = \frac{1}{2}|\psi_+\rangle_R + \frac{1}{\sqrt{2}}|\psi_0\rangle_M + \frac{1}{2}|\psi_-\rangle_L, \quad (15)$$

where

$$|\psi_\pm\rangle = \frac{|\psi_1\rangle + |\psi_2\rangle \pm \sqrt{2}|\psi_3\rangle}{2}, \quad |\psi_0\rangle = \frac{|\psi_1\rangle - |\psi_2\rangle}{\sqrt{2}} \quad (16)$$

are the corresponding qutrit eigenstates with eigenvalues ± 1 and 0. The illustration of this deflection is given in Fig. 4(d). It is interesting to note that $|\psi_3\rangle$ appears either on the left port or the right port, but it never appears on the undeflected middle port. As with the qubit case, the simulations in PPLN are repeated for Λ qutrits of wavelengths $\lambda_1 = 532$ nm, $\lambda_2 = 584$ nm, and $\lambda_3 = 452$ nm, and with pump wavelengths $\lambda_{13} = 3000$ nm and $\lambda_{23} = 2000$ nm. The nonlinear crystal dimensions and pump intensities are as before, with the exception that now the QPM pattern is aperiodic, as explained previously. The simulation results presented in Fig. 5 agree well with the analytic derivation. Slight asymmetries can be explained due to the finite aperture of the pump beam, deforming the transverse gradient in the nonlinear coupling. The analysis of the V and ladder schemes [Figs. 4(b) and 4(c)] results in identical behavior [Eq. (15) and

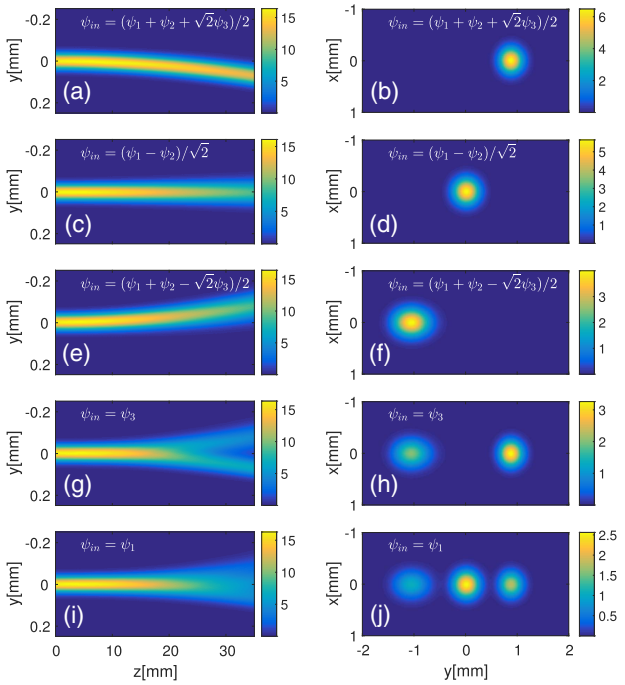

Fig. 5. Simulated photodetection probability in PPLN with a quasi-periodic SG poling pattern (with units mm^{-1} on the left figures and mm^{-2} on the right ones, normalized as in Fig. 3). All input states are Gaussian with a waist of 50 μm. (a), (b) The input state is the first eigenstate $|\psi_{\mathrm{in}}\rangle = |\psi_+\rangle$ and is deflected to the right. (c), (d) The second eigenstate $|\psi_{\mathrm{in}}\rangle = |\psi_0\rangle$ remains undeflected. (e), (f) The third eigenstate, $|\psi_{\mathrm{in}}\rangle = |\psi_-\rangle$, is deflected to the left. In (g), (h), the state $|\psi_{in}\rangle = |\psi_3\rangle$ is projected onto the eigenstates $|\psi_+\rangle$ and $|\psi_-\rangle$ [see Eq. (16)]. The resulting deflection is only to the right or to the left. Finally, (i), (j) show the projection of $|\psi_{in}\rangle = |\psi_1\rangle$ onto all three eigenstates. The resulting far field consists of all three possible deflections.

Fig. 5], with the deflected eigenstates given by the cyclic permutation $(1,2,3) \to (2,3,1) \to (3,1,2)$ on the input frequencies for the Λ, V, and ladder schemes, respectively.

Two-photon bunching can also be manifested in the qutrit case. For two Λ scheme photons in the initial pure state $|\psi_{\mathrm{in}}\rangle = |\psi_1\psi_2\rangle$, the output state is written as

$$|\psi_{\mathrm{out}}\rangle = \frac{1}{2\sqrt{2}}|\psi_+\psi_+\rangle_R - \frac{1}{\sqrt{2}}|\psi_0\psi_0\rangle_M + \frac{1}{2\sqrt{2}}|\psi_-\psi_-\rangle_L + \frac{1}{2}|\psi_+\rangle_R|\psi_-\rangle_L, \tag{17}$$

which is clearly a two-qutrit path-entangled state, demonstrating photon bunching (with the exception of the $|\psi_+\psi_-\rangle$ ket). Note that the $|\psi_0\rangle$ photons are always bunched in the middle output port. As with the qubit case, this spatial separation of orthogonal eigenstates might prove beneficial to quantum information processing using frequency domain qutrits [24–26].

4. CONCLUSIONS

In summary, we have shown that paraxial photons propagating in specially engineered nonlinear media exhibit the properties of 2D quantum particles with internal angular momentum of potentially arbitrary dimension. The couplings between the discrete set of frequencies that satisfy phase-matching constitute the analog of an external magnetic field with which the photons interact. When the coupling varies in space, quantum correlations appear between the spatial and spectral degrees of freedom. For the simpler cases of qubits and qutrits, we investigate the equivalent of an all-optical SG effect for photons, which allows the projection and spatial separation of orthogonal frequency-superposition states. Such an effect is also expected to produce, for example, two-photon entanglement in the frequency domain that resembles the familiar HOM 2002 state [2]. The possible applications for the proposed effect include frequency-basis quantum computing [20]; color-entanglement generation [27] for quantum information and communication protocols, without the necessity to use multiple spatial modes [25] or biphotons [26] for the case of qutrits; two-mode quantum state tomography [28]; and quantum key-distribution protocols, which have been proven to be more secure when using qutrits [24]. The SG deflector, comprising a *single* optical element, can be used in these schemes as a spectral-to-spatial beam splitter (or tritter), being all-optically controlled, as opposed to electronically controlled realizations [6,8,10]. Moreover, the resulting states in SG projection are expected to be robust against fluctuations in the pump pulse area (the latter will alter only the deflection angle), as compared to previous setups that used nonlinear state rotations [2,4].

The concept presented here can be further extended to higher dimensions, using nonlinear photonic crystals that will couple an arbitrary number of optical waves at different frequencies. Moreover, depending on the chosen element of the nonlinear tensor, the interacting modes may have either the same polarization or different polarizations. These generalizations can be done with efficient scalability, as the effect still requires only a single optical element, in contrast to what previous $\chi^{(2)}$ realizations [2,20] can offer. Since frequency-domain qudits are recently gaining attention as possible candidates for carrying quantum information [2–10,20], we are hopeful that this work will help promote such future advancements.

APPENDIX A

The first-order equal-time equal-position correlation function is generally given by $G^{(1)}(\mathbf{r},t;\mathbf{r},t) = \sum_{jk}\langle\psi|E_j^{(-)}(\mathbf{r},t)E_k^{(+)}(\mathbf{r},t)|\psi\rangle$, where jk sum over all interacting frequencies. In experiments, the finite integration time of the detection system is much longer than the optical cycle, thus the field products $E_j^{(-)}E_k^{(+)}$ with different carrier frequencies ($j \neq k$) are averaged out. The only contribution now comes from the diagonal terms [see Eq. (1)]

$$G^{(1)}(\mathbf{r},t;\mathbf{r},t) = \frac{\hbar\bar{v}_g}{2\epsilon_0 nc}\sum_j\langle\psi|\phi_j^\dagger(\mathbf{r},t)\phi_j(\mathbf{r},t)|\psi\rangle,$$

where the prefactor arises from the field quantization in a dielectric medium [13]. Now let $|\psi\rangle$ be a single-photon paraxial wavepacket state $|\psi\rangle = \sum_{\mathbf{q},j}c_{\mathbf{q},j}|1_{\mathbf{k}_j+\mathbf{q}}\rangle$. The SU(2) [or SO(3)] symmetry of our dynamics does not mix $\phi^\dagger$ with ϕ, and therefore we can safely argue that $\langle\psi|\phi_j^\dagger\phi_j|\psi\rangle = \sum_n\langle\psi|\phi_j^\dagger|n\rangle\langle n|\phi_j|\psi\rangle = \langle\psi|\phi_j^\dagger|0\rangle\langle 0|\phi_j|\psi\rangle$. Denoting $\psi_j = \langle 0|\phi_j|\psi\rangle$, and multiplying Eq. (4) with $\langle 0|$ on the left and $|\psi\rangle$ on the right yields the equation

$$i\frac{\partial}{\partial z}\Psi = \left[\frac{1}{2}\mathbf{M}^{-1}\mathbf{p}^2 - \Sigma\cdot\mathbf{B}(\mathbf{r})\right]\Psi,$$

where $\Psi = (\psi_1, \ldots, \psi_N)$ ($N = 2, 3$ in this paper) is a c-number vector. From here the correlation function is readily found:

$$G^{(1)}(\mathbf{r}, t; \mathbf{r}, t) = \frac{\hbar \bar{v}_g}{2\epsilon_0 nc} \sum_j |\psi_j|^2(\mathbf{r}, t) = \frac{\hbar \bar{v}_g}{2\epsilon_0 nc} \Psi^\dagger \Psi(\mathbf{r}, t).$$

Funding. Israel Science Foundation (ISF) (1415/17).

REFERENCES AND NOTE

1. M. O. Scully and M. S. Zubairy, *Quantum Optics* (Cambridge, 2001).
2. T. Kobayashi, R. Ikuta, S. Yasui, S. Miki, T. Yamashita, H. Terai, Y. Takashi, M. Koashi, and N. Imoto, "Frequency-domain Hong–Ou–Mandel interference," Nat. Photonics **10**, 441–444 (2016).
3. C. Joshi, A. Farsi, and A. Gaeta, "Hong-Ou-Mandel interference in the frequency domain," in *Conference on Lasers and Electro-Optics (CLEO): QELS_Fundamental Science* (2017), paper FF2E.3.
4. S. Clemmen, A. Farsi, S. Ramelow, and A. L. Gaeta, "Ramsey interference with single photons," Phys. Rev. Lett. **117**, 223601 (2016).
5. P. Treutlein, "Viewpoint: Photon qubit is made of two colors," Physics **9**, 135 (2016).
6. M. Kues, C. Reimer, P. Roztocki, L. R. Cortes, S. Sciara, B. Wetzel, Y. Zhamg, A. Cino, S. T. Chu, B. E. Little, D. J. Moss, L. Caspani, J. Azana, and R. Morandotti, "On-chip generation of high-dimensional entangled quantum states and their coherent control," Nature **546**, 622–626 (2017).
7. S. Clemmen, R. Van Laer, A. Farsi, J. S. Levy, M. Lipson, and A. Gaeta, "Towards frequency-coded q-dit manipulation using coherent four-wave mixing," in *Conference on Lasers and Electro-Optics (QELS)* (2012), paper QM2H.6.
8. J. M. Lukens and P. Lougovski, "Frequency-encoded photonic qubits for scalable quantum information processing," Optica **4**, 8–16 (2017).
9. P. Imany, O. D. Odele, M. S. Alshaykh, H. H. Lu, D. E. Leaird, and A. M. Weiner, "Frequency-domain Hong–Ou–Mandel interference with linear optics," Opt. Lett. **43**, 2760–2763 (2018).
10. H. H. Lu, J. M. Lukens, N. A. Peters, O. D. Odele, D. E. Leaird, A. M. Weiner, and P. Lougovski, "Electro-optic frequency beam splitters and tritters for high-fidelity photonic quantum information processing," Phys. Rev. Lett. **120**, 030502 (2018).
11. A. Karnieli and A. Arie, "All-optical Stern-Gerlach effect," Phys. Rev. Lett. **120**, 053901 (2018).
12. R. W. Boyd, *Nonlinear Optics* (Academic, 2008).
13. J. C. Garrison and R. Y. Chiao, *Quantum Optics* (Oxford University, 2008).
14. More accurately, these relations are obtained by redefining φ_{12} as $\varphi_{12} \to -\pi/2 - \varphi_{12}$.
15. M. A. M. Marte and S. Stenholm, "Paraxial light and atom optics: the optical Schrödinger equation and beyond," Phys. Rev. A **56**, 2940–2953 (1997).
16. H. Suchowski, D. Oron, A. Arie, and Y. Silberberg, "Geometrical representation of sum frequency generation and adiabatic frequency conversion," Phys. Rev. A. **78**, 063821 (2008).
17. A. Karnieli and A. Arie, "Fully controllable adiabatic geometric phase in nonlinear optics," Opt. Express **26**, 4920–4932 (2018).
18. The nonlinear coupling, κ_{12}, is proportional to the magnitude of the first Fourier component of the poling pattern [12], given by $a_1 = (2/\pi) d_{ij} \sin(\pi D)$, where d_{ij} is the ijth component of the nonlinear susceptibility tensor and D is the poling duty cycle. D can be varied along, say y, such that κ_{12} varies *linearly* with y, by letting $D = (1/\pi) \arcsin(y/W)$, where W is the poled region width. For further details, see Ref. [11].
19. W. Gerlach and O. Stern, "Der experimentelle nachweiss der richtungsquantelung im magnetfeld," Z. Phys. **9**, 349–352 (1922).
20. M. Y. Niu, I. L. Chuang, and J. H. Shapiro, "Qudit-basis universal quantum computation using $\chi^{(2)}$ interactions," Phys. Rev. Lett. **120**, 160502 (2018).
21. T. Ellenbogen, N. Voloch-Bloch, A. Ganany-Padowicz, and A. Arie, "Nonlinear generation and manipulation of Airy beams," Nat. Photonics **3**, 395–398 (2009).
22. A. Arie and N. Voloch, "Periodic, quasi-periodic, and random quadratic nonlinear photonic crystals," Laser Photon. Rev. **4**, 355–373 (2010).
23. R. Lifshitz, A. Arie, and A. Bahabad, "Photonic quasicrystals for nonlinear optical frequency conversion," Phys. Rev. Lett. **95**, 133901 (2005).
24. D. Bruß and C. Macchiavello, "Optimal eavesdropping in cryptography with three-dimensional quantum states," Phys. Rev. Lett. **88**, 127901 (2002).
25. A. Vaziri, G. Weihs, and A. Zeilinger, "Experimental two-photon, three-dimensional entanglement for quantum communication," Phys. Rev. Lett. **89**, 240401 (2002).
26. A. Halevy, E. Megidish, T. Shacham, L. Dovrat, and H. S. Eisenberg, "Projection of two biphoton qutrits onto a maximally entangled state," Phys. Rev. Lett. **106**, 130502 (2011).
27. S. Ramelow, L. Ratschbacher, A. Fedrizzi, N. K. Langford, and A. Zeilinger, "Discrete tunable color entanglement," Phys. Rev. Lett. **103**, 253601 (2009).
28. Y. Shaked, Y. Michael, R. Z. Vered, L. Bello, M. Rosenbluh, and A. Pe'er, "Lifting the bandwidth limit of optical homodyne measurement with broadband parametric amplification," Nat. Commun. **9**, 609 (2018).

132.66.11.211 {ts '2018-10-15 15:17:02'}